SciPost Physics Proceedings — Submission

Effect of the Magnetic Horizon on the Combined Fit of the Pierre Auger Observatory Spectrum and Composition Data

Juan Manuel González[1] [2] **for the Pierre Auger Collaboration** [3†] [*]

1 Instituto Balseiro, UnCuyo, Av. Bustillo 9500, 8400 San Carlos de Bariloche, Argentina
2 CONICET
3 Observatorio Pierre Auger, Av. San Martín Norte 304, 5613 Malargüe, Argentina

† spokespersons@auger.org

22nd International Symposium on Very High Energy Cosmic Ray Interactions (ISVHECRI 2024)
Puerto Vallarta, Mexico, 8-12 July 2024
doi:10.21468/SciPostPhysProc.?

Abstract

We interpret the Pierre Auger Observatory's measurement of the energy spectrum and mass composition of cosmic rays with energies above $10^{17.8}$ eV as coming from two extragalactic source populations, one dominating the flux below a few EeV and the other above. Fitting the data neglecting magnetic fields, we find that the high-energy population is required to have a very hard injection spectrum, incompatible with the expectations from diffusive shock acceleration (E^{-2}). Turbulent magnetic fields between us and the closest sources can suppress the flux of low-rigidity particles, modifying the cosmic-ray spectrum at Earth. We include the effect of magnetic fields in the fit to the Auger data, which results in softer high-energy injection spectra.

Received Date
Accepted Date
Published Date

Contents

*Full author list at http://www.auger.org/archive/authors_2024_06.html.

---

1 Introduction

The Pierre Auger Observatory's measurements of cosmic ray (CR) flux and the depth of shower maximum (X_{max}) distributions are useful to constrain the characteristics of CR sources [1–3]. Two distinct source populations are needed to explain observations above $10^{17.8}$ eV. The first, known as the low-energy component (L), dominates at energies below a few EeV. The second, the high-energy component (H), prevails at higher energies. When these populations are modelled as continuously distributed equal luminosity sources injecting a mixed mass composition with power-law spectra and rigidity-dependent cutoffs, a maximum likelihood fit suggests that the spectrum of the high-energy component's is significantly harder than expected from diffusive shock acceleration theories [4] .

The presence of intergalactic magnetic fields, coupled with the finite separations between sources, may cause a diminished flux of low-energy particles when the diffusion times from even nearby sources exceeds their lifetimes. This results in a suppression of the observed spectrum, thus changing the deduced source injection spectrum. This study explores the relevant magnetic field properties and cosmic ray source characteristics to determine when this phenomenon becomes significant, potentially altering the interpretation of observed data.

1.1 Modelling the sources

In this work, we describe the injection rates of cosmic ray (CR) sources per unit volume and time for particles with mass number A, energy E, and charge Z with the following expression,

$$\dot{Q}_{A,x}(z,E) = \dot{Q}_{0,x} f_{A,x} \times \left(\frac{E}{E_0}\right)^{-\gamma_x} F_{\text{cut}}\left(\frac{E}{ZR_{\text{cut}}^x}\right), \tag{1}$$

where the index x indicates either the low-energy (L) or high-energy (H) population. Here, $\dot{Q}_{0,x}$ acts as a normalisation factor that fixes the differential CR emission rate at a reference energy E_0, which is much lower than the hydrogen cutoff energy R_{cut}^x. In this analysis, we assume the sources primarily inject five elements: hydrogen (H), helium (He), nitrogen (N), silicon (Si), and iron (Fe). The relative abundances of elements with mass A from the sources are represented by $f_{A,x}$. The rigidity cutoff function, F_{cut}, limits the particle flux at energies greater than ZR_{cut}^x. We parametrize it using a hyperbolic secant profile $F_{\text{cut}}(x) = \text{sech}(x^{\Delta})$, where Δ controls the sharpness of the suppression, considering Δ values of 1, 2, and 3.

We simulate the particles' propagation from the sources towards Earth with the SimProp software [9]. The arrival flux depends on the nuclear photo-disintegration cross sections (for which we use information obtained from TALYS) as well as on the extragalactic background light (we assume the Gilmore et al. [11] model). There is an additional dependence on the hadronic interactions model used to account for the X_{max} measurements. The present work studies the effect of using both EPOS-LHC [12] and Sibyll 2.3d [13] to interpret the data.

We categorise nuclei arriving at Earth by their mass number: $A = 1$ for H, 2–4 for He, 5–16 for the N group, 17–30 for the Si group, and all the other masses up to 56 form the Fe group. Nuclei that reach Earth without changing their original mass group are labeled as *primary nuclei*. In contrast, nuclei that undergo photo-disintegration and end up in a different mass group from their original production are classified as *secondary nuclei*.

1.2 Magnetic horizon effect

For large enough inter-source distances d_s (the source density $n_s = 1/d_s^3$ is low) and a strong enough magnetic field, low-energy particles that propagate diffusively won't have enough time to reach us even from nearby sources, which leads to a low-energy suppression of the flux [5, 14, 15]. This effect is called the magnetic horizon effect (MHE).

We model the extragalactic magnetic field EGMF as turbulent and isotropic, described by the root mean squared amplitude $B_{\rm rms}$ and the coherence length $L_{\rm coh}$. A critical energy can be defined as that for which the Larmor radius of a particle equals $L_{\rm coh}$, which for nuclei with atomic number Z is $E_{\rm crit} \equiv ZR_{\rm crit}$, with $R_{\rm crit} \equiv |e|B_{\rm rms}L_{\rm coh} \simeq 0.9(B_{\rm rms}/{\rm nG})(L_{\rm coh}/{\rm Mpc})$ EeV.

The flux reaching Earth in the presence of EGMFs can be obtained by multiplying the one resulting from propagation in the absence of magnetic fields by an energy-dependent suppression factor [16, 17],

$$J(E) \equiv G(E/E_{\rm crit}) J_{B=0}(E), \text{ and } \qquad G(x) = \exp\left[-\left(\frac{a X_s}{x + b\,(x/a)^{\beta}}\right)^{\alpha}\right], \tag{2}$$

where $X_s = d_s/\sqrt{r_H L_{\rm coh}}$, with $r_H = c/H_0$ the Hubble radius. The parameters α, β, a and b depend on whether particles are primary or secondary nuclei and on the spectral index of the sources [17]. Considering magnetic field amplitudes in the range $4\,{\rm nG} < B_{\rm rms} < 100\,{\rm nG}$ and coherence lengths such that $25\,{\rm kpc} < L_{\rm coh} < 1\,{\rm Mpc}$, one would expect the critical rigidity to lay $0.1\,{\rm EeV} < R_{\rm crit} < 100\,{\rm EeV}$. Also, if $3\,{\rm Mpc} < d_s < 40\,{\rm Mpc}$ ($10^{-5} \lesssim n_s/{\rm Mpc}^{-3} \lesssim 3\times10^{-2}$), we have $0.05 < X_s < 4$. We will thus constrain the parameters $R_{\rm crit}$ and X_s within these ranges.

We assume that the L component source population has a larger density, such that the magnetic horizon effect can be neglected for this component. That is, the MHE only modifies the H component. We also neglect the Galactic contribution to the CR flux above $10^{17.8}$ eV.

2 Combined Fit to the spectrum and $X_{\rm max}$ distributions

We fit the spectral data from [6] above $10^{17.8}$ eV, using logarithmic energy bins of width $\Delta \log_{10} E = 0.1$. Additionally, we analyse the $X_{\rm max}$ distributions provided in [7], with bins of $\Delta X_{\rm max} = 20\,{\rm g\,cm^{-2}}$ for each energy bin. To model the source injection spectra, we use Eq. 1, taking into account energy losses due to redshift and interaction effects. We also include the magnetic horizon effect (MHE) multiplying the spectrum at Earth by the suppression factor G (Eq. 2). The best-fit parameters arise from maximizing the likelihood function, as described in [8]. This likelihood consists of two parts: one for the energy spectrum, modelled as a product of Gaussian distributions across the energy bins; and another for the $X_{\rm max}$ distributions, represented by multinomial distributions modelled with Gumbel functions. The parameters of the former depends on the hadronic interaction model. Since these two measurements are statistically independent, the total likelihood is the product of the energy spectrum and $X_{\rm max}$ likelihoods. The likelihood is a function the parameters γ_x, $R^x_{\rm cut}$, and the element fractions $f_{A,x}$ for both populations. Two additional parameters, X_s and $R_{\rm crit}$, describe the suppression caused by the magnetic horizon. We report the deviance $D = -2\ln(\mathcal{L}/\mathcal{L}_{\rm sat})$, where $\mathcal{L}$ is the likelihood of the model and $\mathcal{L}_{\rm sat}$ corresponds to a perfectly fitting model.

Table 1 shows the fit results for the different cutoff shapes and for the EPOS-LHC and Sybill2.3d hadronic interaction models. Sharper cutoffs (larger Δ) lead to softer H spectra and higher rigidity cutoff $R^{\rm H}_{\rm cut}$. Ignoring the MHE results in $\gamma_H < 1$ for all cases. Changing the hadronic model from EPOS-LHC to Sibyl2.3d results in softer H and harder L spectra. In all cases, the L rigidity cutoff is degenerated above about 40 EeV.

Including the MHE, for $\Delta = 1$, the fit still favours a scenario with no EGMF. For steeper cutoffs, the best fit has a sizeable MHE, resulting in $\gamma_H > 1$. For Sibyl2.3d with $\Delta = 3$, we find

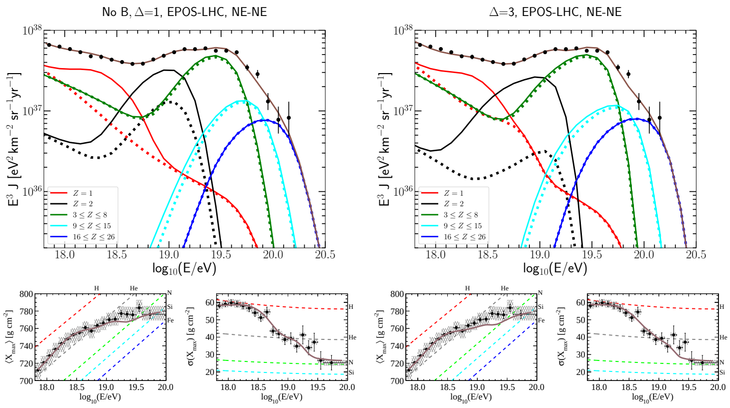

Figure 1: Flux at Earth (upper panels) and moments of the $X_{\rm max}$ distribution (lower panels), for EPOS-LHC model. In the top panels, the dotted lines show the primary nuclei's flux, while solid lines do so for whole (primary plus secondary) mass group. The left column presents results for a $\Delta = 1$ cutoff (no MHE preferred), while the right column corresponds to a $\Delta = 3$ cutoff, where the MHE plays an important role.

that $\gamma_H = 2$, consistent with the expectations from diffusive shock acceleration (DSA). This scenario does not have the best deviance, but this may change when considering experimental systematic uncertainties.

	EPOS-LHC							Sybill2.3d						
Δ	$\gamma_{\rm H}$	$R^{\rm H}_{\rm cut}$ [EeV]	$\gamma_{\rm L}$	$R^{\rm L}_{\rm cut}$ [EeV]	X_s	$R_{\rm crit}$ [EeV]	D (N=353)	$\gamma_{\rm H}$	$R^{\rm H}_{\rm cut}$ [EeV]	$\gamma_{\rm L}$	$R^{\rm L}_{\rm cut}$ [EeV]	X_s	$R_{\rm crit}$ [EeV]	D (N=353)
	no EGMF													
1	−2.19	1.35	3.54	> 60	—	—	572	−1.67	1.42	3.36	2.21	—	—	660
2	0.16	5.75	3.65	> 52	—	—	605	0.51	5.96	3.53	> 27	—	—	661
3	0.56	7.41	3.75	> 41	—	—	651	0.81	7.49	3.64	> 29	—	—	699
	with EGMF													
1	-2.19	1.35	3.54	>60	0	—	572	-1.67	1.42	3.37	2.21	0	—	660
2	1.03	6.02	3.62	> 51	> 3.2	1.97	583	1.35	6.22	3.53	> 25	> 3.1	1.54	635
3	1.43	7.50	3.69	> 61	2.8	2.79	614	2	7.50	3.62	> 31	2.6	3.77	640

Table 1: Parameters of the fit for the EPOS-LHC and Sybill2.3d hadronic interaction models and different steepness of the cutoff $\Delta = 1$, 2 or 3. The first three rows do not include the magnetic horizon effect, while the last three rows do.

Fig 1 presents the results for the spectrum at Earth and the first two $X_{\rm max}$ moments for two cutoff shapes and the EPOS-LHC hadronic model. Some general features are common for both scenarios. Firstly, the composition becomes heavier for increasing energy. Most low-energy protons and He nuclei arise from the photo-disintegration of nitrogen. The instep feature is mostly due to a bump in the He flux and an increase in the N contribution. Above the instep, the flux is dominated by N up to the high-energy suppression (around $\sim 50\,$EeV). For higher energies, we find mostly Si and Fe nuclei.

2.1 Effect of systematic uncertainties

Experimental systematic uncertainties on the energy scale and $X_{\rm max}$ calibration can affect the fit results. An energy scale uncertainty $\Delta E/E = \pm 14\%$ is considered [6]. The systematic uncertainties on the measured $X_{\rm max}$ depend on the energy, ranging from 6 to 9 $\rm g\,cm^{-2}$ [18]. To quantify the effects of these uncertainties, we shifted both measurements one systematic uncertainty up or down and carried out the fit again, having nine possible shift combinations. The results for the deviance and γ_H are shown in Fig. 2 for two scenarios providing the best fit case without MHE (EPOS-LHC with $\Delta = 1$) and with MHE (Sibyll2.3d with $\Delta = 3$). The

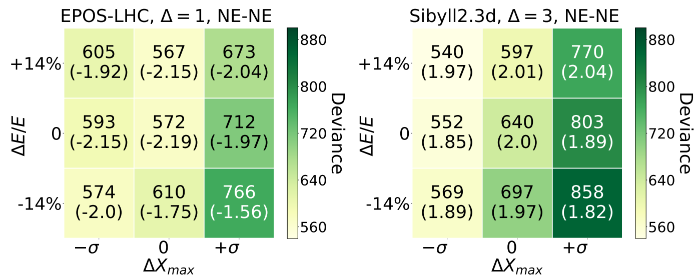

Figure 2: Deviance and $\gamma_{\rm H}$ (in parenthesis) after performing shifts of $\pm\sigma_{\rm sys}$ in the energy and $X_{\rm max}$ scales.

smaller deviance results for the last case with a positive shift in energy and a negative one in $X_{\rm max}$ and with $\gamma_H \simeq 2$. The magnetic field parameters satisfy $X_{\rm s} R_{\rm crit} \simeq 5\,{\rm EeV}$.

3 Conclusions

Carrying out a combined fit to the spectrum and composition data measured by the Pierre Auger Observatory above $10^{17.8}$ eV, while neglecting the possible effect of extragalactic magnetic fields requires very hard injection spectra for the H component, with $\gamma_{\rm H} < 1$. The results strongly depend on the assumed hadronic model and cutoff shape, with the spectrum softening and the deviance increasing for sharper cutoffs. For these kind of scenarios, the best-fit results for EPOS-LHC with $\Delta = 1$, where $\gamma_{\rm H} \approx -2.2$.

When we do include the effect of magnetic fields, we found that cases with sharper cutoffs have softer high-energy spectra with $\gamma_H > 1$ and with lower deviances than their no-EGMF counterpart, regardless of the hadronic model considered. In particular, for a $\Delta = 3$ cutoff with Sibyll2.3d, we obtained a $\gamma_H = 2$. We found that when the MHE effect plays a relevant role to model the soectrum, the approximate relation $X_{\rm s} R_{\rm crit} \simeq 5$ to 10 EeV should hold, where these quantities are related through

$$X_{\rm s} R_{\rm crit} \simeq 5\ {\rm EeV} \frac{d_{\rm s}}{20\,{\rm Mpc}} \frac{B_{\rm rms}}{50\,{\rm nG}} \sqrt{\frac{L_{\rm coh}}{100\,{\rm kpc}}}. \tag{3}$$

Thus, large mean inter-source distances (20 Mpc or more) and large EMGFs amplitudes in the region between us and the closest sources are required to achieve the suppression.

References

[1] A. Aab *et al.* [Pierre Auger Collaboration], *Combined fit of spectrum and composition data as measured by the Pierre Auger Observatory*, JCAP **04**(2017)038, doi:10.1088/1475-7516/2017/04/038.

[2] E. Guido (for the Pierre Auger Collaboration), *Combined fit of the energy spectrum and mass composition across the ankle with the data measured at the Pierre Auger Observatory*, PoS(ICRC2021), **311**, doi:10.22323/1.395.0311 .

[3] A. Abdul Halim *et al.* [Pierre Auger Collaboration], *Constraining the sources of ultra-high-energy cosmic rays across and above the ankle with the spectrum and composition data*

measured at the Pierre Auger Observatory, JCAP, **05**, 024, (2023), doi:10.1088/1475-7516/2023/05/024.

[4] E. Fermi, *On the Origin of the Cosmic Radiation*, Phys. Rev., **75**, 1169–1174, (1949), doi:10.1103/PhysRev.75.1169.

[5] R. Aloisio and V. Berezinsky, *Diffusive Propagation of Ultra-High-Energy Cosmic Rays and the Propagation Theorem*, Astrophys. J. **612** (2004), 900, doi:10.1086/421869.

[6] P. Abreu *et al.* [Pierre Auger Collaboration], *The energy spectrum of cosmic rays beyond the turn-down around* 10^{17} eV *as measured with the surface detector of the Pierre Auger Observatory*, Eur. Phys. J. C, **81**, (2021), 966 doi:10.1140/epjc/s10052-021-09700-w.

[7] A. Yushkov (for the Pierre Auger Collaboration), *Mass Composition of Cosmic Rays with Energies above* $10^{17.2}$ eV *from the Hybrid Data of the Pierre Auger Observatory*, PoS(ICRC2019), **482**, doi:10.22323/1.358.0482.

[8] A. Abdul Halim *et al.*, Pierre Auger Collaboration, *Impact of the magnetic horizon on the interpretation of the Pierre Auger Observatory spectrum and composition data*, JCAP **07**, 094 (2024), doi:10.1088/1475-7516/2024/07/094.

[9] R. Aloisio *et al.*, *SimProp: a Simulation Code for Ultra High Energy Cosmic Ray Propagation*, JCAP 11, (2017), 009, doi:10.1088/1475-7516/2012/10/007.

[10] A.J. Koning, S. Hilaire and M.C. Duijvestijn, *TALYS: Comprehensive Nuclear Reaction Modeling*, American Institute of Physics Conference Series. **769**, (2005), 1154, doi:10.1063/1.1945212.

[11] R. C. Gilmore, R. S. Somerville, J. R. Primack, A. Domínguez, *Semi-analytic modelling of the extragalactic background light and consequences for extragalactic gamma-ray spectra*, arXiv, **1212.5866**, doi:10.1111/j.1365-2966.2012.20841.x.

[12] T. Pierog *et al.*, *POS LHC: Test of collective hadronization with data measured at the CERN Large Hadron Collider*, Phys. Rev. C, **92**, (2015), 034906, doi:10.1103/PhysRevC.92.034906.

[13] F. Riehn, R. Engel, A. Fedynitch, T. K. Gaisser and T. Stanev, *Hadronic interaction model Sibyll 2.3d and extensive air showers*, Phys. Rev. D, **102**, (2020), 063002, doi:10.1103/PhysRevD.102.063002.

[14] D. Wittkowski (for the Pierre Auger Collaboration), *Reconstructed properties of the sources of UHECR and their dependence on the extragalactic magnetic field*, PoS (ICRC2017), 563, doi:10.22323/1.301.0563 .

[15] S. Mollerach and E. Roulet, *Extragalactic cosmic rays diffusing from two populations of sources*, Phys. Rev. D, **101**, (2020), 103024, doi:10.1103/PhysRevD.101.103024.

[16] S. Mollerach and E. Roulet, *Magnetic diffusion effects on the ultra-high energy cosmic ray spectrum and composition*, JCAP **10**(2013)013, doi:10.1088/1475-7516/2013/10/013.

[17] J. González, S. Mollerach and E. Roulet, *Magnetic diffusion and interaction effects on ultrahigh energy cosmic rays: Protons and nuclei*, Phys. Rev. D, **104**, (2021), 063005, doi:10.1103/PhysRevD.104.063005

[18] A. Aab et al. (Pierre Auger Collaboration), *Depth of Maximum of Air-Shower Profiles at the Pierre Auger Observatory: Measurements at Energies above* $10^{17.8}$ eV, Phys. Rev. D, **90**, (2014), 122005, doi:10.1103/PhysRevD.90.122005